Jurnal Polimesin
Department of Mechanical Engineering
State Polytechnic of Lhokseumawe
http://e-jurnal.pnl.ac.id/polimesin
e-ISSN : 2549-1999 No. : 2 Month : April
p-ISSN : 1693-5462 Volume : 24 Year : 2026

Processing dates: received on 2025-11-09, reviewed on 2026-02-10, accepted on 2026-03-03 and online availability on 2026-04-25

Optimization of hybrid carbon–bamboo composite structure based on flexural test and finite element simulation for UAV wing spar

Muhammad Nuzan Rizki[1,*], Asnawi[1], Iqbal Kamar[2], Maulana Agil Ibrahim[1]
[1]Department of Mechanical Engineering, University of Malikussaleh, Lhokseumawe 24353, Indonesia
[2]Department of Chemical Engineering, University of Malikussaleh, Lhokseumawe 24353, Indonesia
*Corresponding Author: mnuzanrizki@unimal.ac.id

Abstract

The structural performance of Unmanned Aerial Vehicle (UAV) wing spars demands a balance between high strength and adequate stiffness. This study investigates the optimal configuration of bamboo–carbon fiber hybrid composites and evaluates the suitability of different spar cross-section geometries through experimental flexural testing, Taguchi-based statistical optimization, and Finite Element Method (FEM) simulation. Nine composite variations were fabricated and tested in accordance with ASTM D7264, employing three control factors: volume fraction, fiber ratio, and stacking sequence. The experimental results indicated that variation V7 (60% total fiber volume, 40:60 bamboo–carbon ratio, CBC stacking sequence) demonstrates the highest mechanical performance, achieving a flexural strength of 288.5 MPa and a flexural modulus of 31.8 GPa, which was further supported by the highest Signal-to-Noise (S/N) ratios for both responses. The optimum material configuration was subsequently applied to FEM simulations of three spar cross-sectional geometries. The results revealed that the hollow circular profile exhibited a limited safety margin (SF = 1.09), whereas the W-shaped and hollow-square profiles achieved higher safety factors of 2.15 and 2.18, respectively. Among the evaluated designs, the hollow-square spar provides the most favorable structural response, characterized by lower maximum stress, reduced deflection, and the highest safety margin.

Keywords:
Hybrid composites, natural-synthetic fibers, design optimization, spar structure cross-section, UAV

1 Introduction

The drone market in Southeast Asia is projected to grow at an estimated rate of 5.75% between 2025 and 2029 [1]. As the most populous country in the region, Indonesia holds significant potential to position itself as a key player in this emerging industry. The rapid expansion of drone adoption across various sectors, including industrial manufacturing, agriculture, plantations, and fisheries, further strengthens this opportunity [2-4].

One well-known type of drone is the Unmanned Aerial Vehicle (UAV). In the development of this type of drone technology, structural efficiency is a key factor in increasing productivity. Previous research has extensively discussed strategies for improving efficiency by reducing the weight of these UAVs [5-10]. However, these studies still focus on the use of synthetic fiber-based composites as reinforcement. This material offers high mechanical strength performance but suffers from the drawbacks of high production costs and non-renewability.

On the other hand, the combination of synthetic and natural fibers as reinforcement for composite materials is an alternative that is more environmentally friendly and economical while still providing adequate mechanical strength [11-17]. Furthermore, studies examining natural-synthetic fiber hybrid composites for UAV structural applications are still limited and require further study.

Despite the growing body of research on hybrid natural–synthetic fiber composites, most existing studies primarily focus on material-level characterization rather than their integration into real structural components. Furthermore, investigations on UAV wing spars predominantly employ fully synthetic composites, leaving the structural feasibility of sustainable hybrid materials insufficiently explored. To the authors' knowledge, limited studies have systematically combined statistical optimization and numerical validation to evaluate both material configuration and structural geometry for UAV spar applications.

Therefore, this study proposes a novel integrated framework that combines Taguchi-based experimental optimization with finite element simulation to identify the most effective bamboo–carbon hybrid composite configuration and apply it to multiple spar cross-sectional designs. The hybrid laminate configurations evaluated in this study include Bamboo–Carbon–Bamboo (BCB), Bamboo–Carbon–Carbon (BCC), and Carbon–Bamboo–Carbon (CBC) stacking sequences, where each notation represents the fiber arrangement through the laminate thickness. This approach not only evaluates the mechanical performance of the hybrid composite but also bridges the gap between material development and structural implementation for lightweight UAV applications.

2 Research method

This study uses an experimental approach to test the flexural mechanical properties of a UAV spar structure made from a carbon fiber-reinforced bamboo fiber composite. After obtaining empirical results from the flexural tests, numerical modeling and simulations were conducted using the Finite Element Method (FEM). The entire research process is illustrated in the research flowchart (Fig. 1).

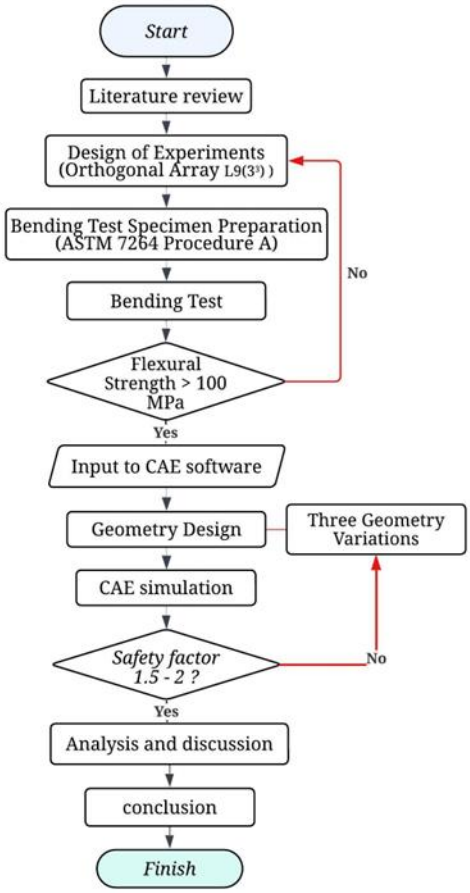

Fig. 1. Research methodology framework

2.1 Design of Experimental (DoE)

The DoE statistical method approach was implemented to efficiently and measurably determine test combinations. The goal was to accurately represent each combination of factors and test the effects of interactions between factors. This allowed for statistical analysis. Therefore, the L9(3^3) orthogonal array was mathematically constructed to allow for balanced testing of all factor and level combinations, without having to try all full combinations (Table 1).

Table 1. A combination of test specimens based on an orthogonal array

Variations	Volume fraction	Fiber ratio		Stacking sequence
		Bamboo	Carbon	
V1	40%	55%	45%	BCB
V2	40%	40%	60%	BCC
V3	40%	25%	75%	CBC
V4	50%	55%	45%	BCC
V5	50%	40%	60%	CBC
V6	50%	25%	75%	BCB
V7	60%	55%	45%	CBC
V8	60%	40%	60%	BCB
V9	60%	25%	75%	BCC

The stacking sequence in carbon fiber–bamboo hybrid composites is an important factor that influences the mechanical properties of the composite, especially in resisting bending loads [18], [19]. In this study, each specimen was composed of three main parts (lamina), each of which could be a layer of bamboo fiber (B) or carbon fiber (C). The stacking sequence was expressed in notations such as BCB, BCC, or CBC, indicating the stacking sequence from the top to the bottom surface of the specimen.

2.2 Specimen preparations

Test specimens were fabricated in accordance with the flexural test specimen standard outlined in ASTM D7264 Procedure A. This standard regulates the dimensions, shape, and testing procedures. The primary materials used were bamboo fiber (*Gigantochloa apus*) obtained from local waste in Lhokseumawe. Plain-weave 3K carbon fiber (density: 0.8 g/cm^3) was obtained from a local e-commerce store, and epoxy resin (density: 1.16 g/cm^3) from Winbond Materials Co., Ltd. served as the binding matrix.

The initial step involved sorting and cleaning the bamboo fibers from the culms. They were then dried until their moisture content stabilized to avoid affecting the resin impregnation process. Simultaneously, the carbon fibers were cut to the mold size and prepared according to the number of layers to be used in each stacking sequence.

After the fibers were laid out, a mixture of epoxy resin and hardener was evenly poured onto each layer at a predetermined mixing ratio (Fig. 2). The fabrication methods used included hand lay-up and vacuum bagging to ensure even resin distribution and minimize voids.

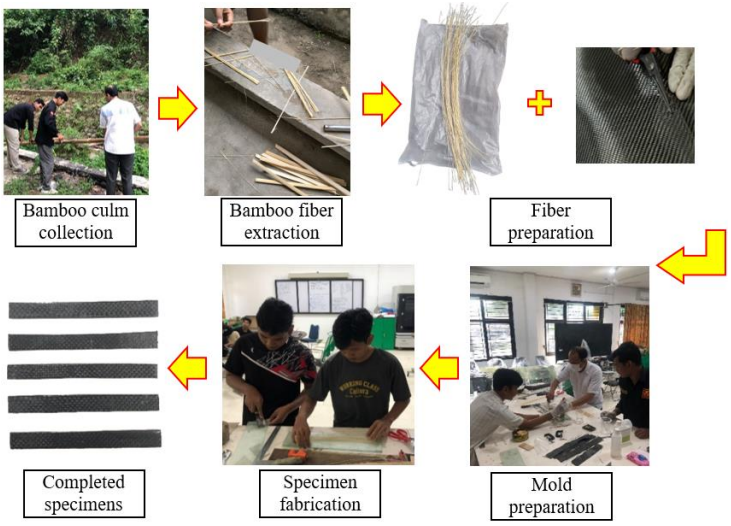

Fig. 2. Hybrid composite specimen manufacturing process

The specimens were then allowed to harden at room temperature. After the curing process was complete, the composite sheets were cut using precision cutting tools to meet the ASTM D7264 standard dimensions of 127 mm in length, 13 mm in width, and 3.2 mm in thickness

2.3 Testing setup

A 3-point flexure test procedure was used in this test. Each combination was repeated five times, resulting in a total of 45 specimens tested. A Hung Ta Instrument Type 3502 Universal Tensile Machine (UTM) was used for the bending tests. The entire test procedure was carried out in accordance with point 11 of ASTM D7264.

2.4 Mechanical analysis

Each material combination produces force (P) and deflection (δ) data that are continuously recorded by the testing machine. All measurements are entered in SI units (force in *N*, length in *mm*). Flexural strength values are calculated using the standard equation for a three-point test (Eq. (1)).

$$\sigma = \frac{3PL}{2bh^2} \tag{1}$$

where σ is stress at the outer surface at mid-span (MPa), P is the applied force (N), L *is* the support span (mm), b *is* the width of the beam (mm), and h *is* the thickness of the beam (mm). The bending strain value on the outer fiber strain is calculated by Eq. (2), where ϵ is the maximum strain at the outer surface (mm/mm), δ is the mid-span deflection (mm).

$$\epsilon = \frac{6\delta h}{L^2} \tag{2}$$

Where P is the measured force (N), L is the span distance (mm), b is the specimen width (mm), h is the specimen thickness (mm), and δ is the deflection at the midpoint (mm). The flexural modulus is determined at the initial linear region of the stress–strain curve. Two approaches are used: (a) the slope (tangent) modulus of the load–deflection curve, which is then converted to a flexural modulus according to ASTM, or (b) the chord modulus calculated from the ratio of the change in stress to the change in strain over a given linear interval (Eq. (3)), where E_f^{chord} *is* the flexural chord modulus of elasticity (MPa).

$$E_f^{chord} = \frac{\Delta\sigma}{\Delta\epsilon} \tag{3}$$

Finally, the flexural strength, flexural modulus, and stress-strain curve parameters were obtained**,** which became the basis for Taguchi analysis, determination of the S/N ratio, and material input for subsequent FEM simulations.

2.5 Taguchi method

The test results were then analyzed using the Taguchi statistical method using statistical software. This method was chosen because it allows for the identification of the factors and levels that most influence flexural strength [20]. Through this approach, each combination of factors and levels tested can be systematically analyzed to determine their relative influence on the test response. Furthermore, the Taguchi method provides efficiency in the number of experiments required, as only a subset of combinations is tested while still being able to statistically represent the full range of parameter variations. This analysis not only identifies the dominant factors but also helps determine the optimal conditions that produce the highest response to the flexural strength of the composite [21]. To quantify the relative influence of each factor on the flexural strength response, the Taguchi analysis in this study uses the normalized value (Eq. (4)) and Multi-Performance Index (MPI) (Eq. (5)), where S *is* the S/N ratio obtained from the Taguchi analysis, N_i *is* the S/N ratio value for the i-th experimental run, N_{min} *is* the minimum S/N ratio among all experimental results, N_{max} *is* the

maximum S/N ratio among all experimental results, ω_1, ω_2 *are* weighting factors assigned to each performance response, and N_1, N_2 *are the* normalized values of the first and second performance criteria.

$$Normalized\ value = \frac{\frac{S}{N_i} - \frac{S}{N_{min}}}{\frac{S}{N_{max}} - \frac{S}{N_{min}}} \quad (4)$$

$$MPI = w_1 \times N_1 + w_2 \times N_2 \quad (5)$$

2.6 Finite element modeling and simulation

Three geometric models were developed and compared to determine the optimal spar configuration, including hollow circular, hollow square, and W-shaped cross-sections (Fig. 3). The hybrid bamboo–carbon composite laminate was modeled as an orthotropic material, with the material axes aligned with the primary fiber direction. The elastic properties used in the simulation were obtained from experimental characterization and are presented in Section 3.

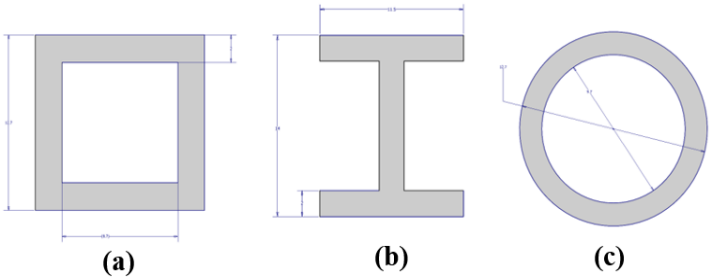

Fig. 3. Spar cross-sectional geometric models: (a) Hollow square, (b) W-shape, and (c) Hollow circular

A static structural analysis was conducted under linear elastic assumptions with small deformation. The laminate was assumed to be perfectly bonded, with no interfacial delamination considered during loading. The spar was constrained at the center to represent the clamping condition of the UAV fuselage, while two upward vertical forces of 142 N were applied at both ends of the span.

A hexahedral mesh was employed due to its suitability for orthotropic composite materials, resulting in approximately 18,676–32,016 elements and 118,854–181,621 nodes. Furthermore, nonlinear contact was defined between the loading tip and the specimen to improve the accuracy of load transfer during the simulation.

3 Results and discussion

This section presents and discusses the results obtained from both the experimental and numerical analyses. The experimental investigation includes the fabrication and flexural testing of hybrid carbon–bamboo composite specimens, which aim to determine the material's flexural strength and stiffness characteristics. The resulting data are then analyzed using the Taguchi statistical method to identify the most influential parameters affecting the bending performance.

Furthermore, the optimal material configuration obtained from the experimental phase is applied to the spar model, which is subsequently analyzed through the FEM to evaluate its structural behavior under loading conditions. The outcomes from the simulation are compared and interpreted to determine the optimal spar design in terms of the highest safety factor.

3.1 Specimen fabrication results

Hybrid composite specimens were fabricated according to the orthogonal array presented in Table 1, which includes variations in fiber volume fraction, bamboo fiber to carbon ratio, and stacking sequence. The fabrication process resulted in nine different combinations. Visual inspection of the specimens revealed minimal surface defects and uniform resin distribution, as shown in Fig. 4.

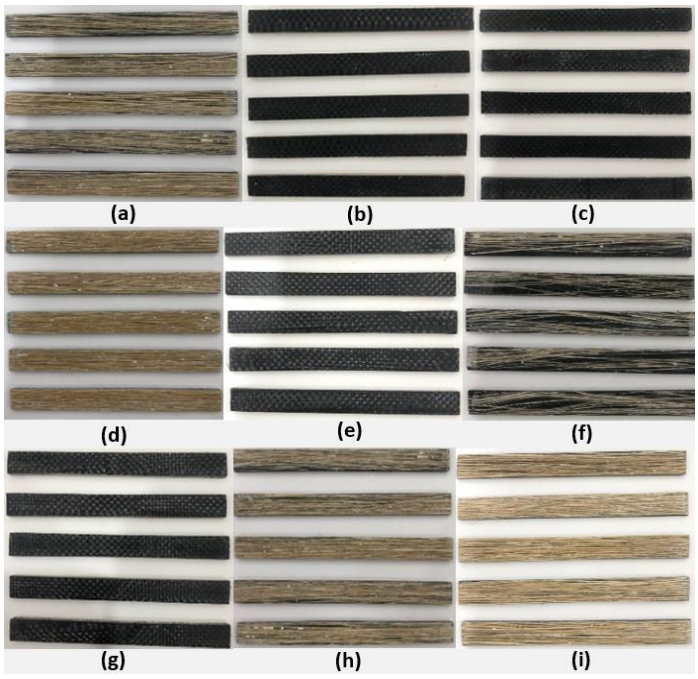

Fig. 4. Fabrication results of carbon fiber–bamboo hybrid composite specimens for nine combination variations (a–i)

3.2 Flexural properties

Flexural testing was conducted according to the ASTM D7264 standard using a three-point flexural configuration. Each specimen was tested with a span-to-thickness ratio of 32:1. Force and deflection data recorded by the UTM were used to calculate the flexural stress, strain, and flexural modulus of each specimen. Fig. 5 shows the overall results of the specimens that had undergone flexural failure.

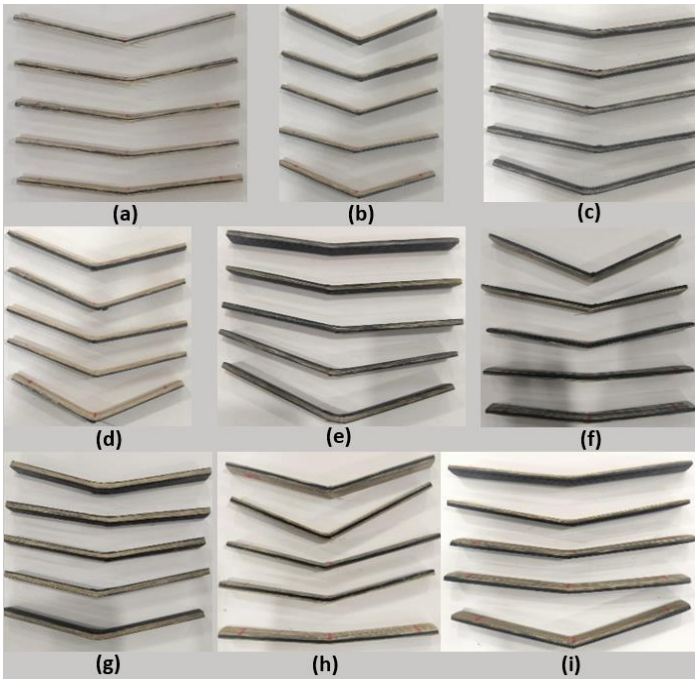

Fig. 5. Results of three-point flexural testing on nine variations of carbon fiber–bamboo hybrid composite specimens (a–i)

All specimens exhibited a maximum tensile strain point at the bottom edge. The observed failure mode was tensile-side fiber rupture [22], [23], where the fibers on the bottom surface experience fracture due to maximum tensile strain, while the top surface only shows cracks in the matrix without total failure. This phenomenon is accompanied by partial delamination in the center area of the specimen.

Flexural strength is commonly used to evaluate a material's ability to withstand deformation due to bending loading until failure occurs. This value indicates the maximum stress that occurs in the outermost fibers of a specimen when subjected to bending loads.

Based on the results of flexural testing on composite materials, with nine combinations of volume fraction, fiber ratio, and arrangement, the flexural behavior of the specimens can be observed as shown in Fig. 6.

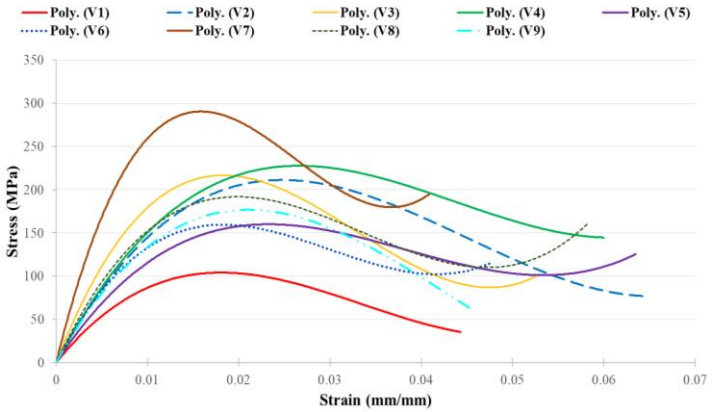

Fig. 6. Representative flexural stress–strain curves of hybrid carbon–bamboo composites

The flexural stress–strain curves for nine specimen variations are shown in Fig. 6. The test data were then processed and displayed in the form of curves using a third-order polynomial approach. The use of the third-order polynomial method was chosen because it is able to provide a smooth and continuous representation of the experimental data, so it can describe the general tendency of material behavior during the flexural loading process well, without eliminating key characteristics such as the maximum flexural strength point and post-peak behavior [24]. Fig. 6 shows a consistent general pattern across all specimen variations, starting from a linear elastic zone at low strain, where stress increases proportionally to strain. At this stage, the fibers and matrix still act cooperatively without internal damage, so the slope of the curve reflects the flexural elastic modulus of each configuration. The gradient differences between variations are primarily influenced by the ratio of carbon fiber to bamboo and the laminate structure, with specimens with higher carbon fiber content exhibiting greater flexural stiffness.

The peak point on the curve marks the onset of material failure, with maximum stress values differing across specimen variations. Variant V7 exhibited the highest flexural strength, followed by V4 and V2, attributed to the higher carbon fiber content and the laminate configuration that more effectively resists bending loads. After passing the peak stress, all specimens experienced a gradual stress decrease (post-peak softening), indicating a progressive failure mode such as delamination and gradual failure of the matrix-fiber bond. This indicates that the hybrid composite does not undergo abrupt brittle failure but retains some residual strength, although its value is highly dependent on the fiber ratio and laminate architecture.

The quantitative values of the flexural properties of the nine test variations are presented in Fig. 7 and Table 2.

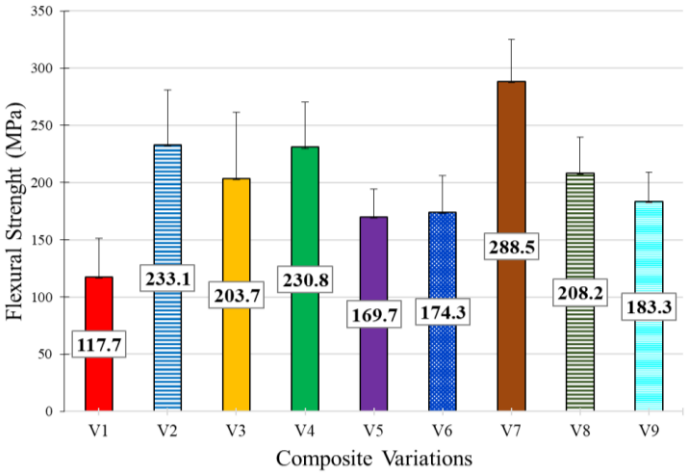

Fig. 7. Flexural properties of the material from nine variations of test specimens

Table 2. Quantitative flexural test data

Variants	Flexural strength (MPa)	Flexural modulus (GPa)	Strain (%)	SNR A (dB)	SNR B (dB)
V1	117.7	4.2	1.9	41.41	12.46
V2	233.1	5.7	3.1	47.35	15.11
V3	203.7	27.3	0.6	46.17	28.72
V4	230.8	6.9	3.0	47.26	16.77
V5	169.7	23.2	0.8	44.59	27.30
V6	174.3	6.7	1.5	44.82	16.52
V7	288.5	31.8	3.3	49.20	30.04
V8	208.2	8.2	1.7	46.36	18.27
V9	183.3	4.9	2.3	45.26	13.80

The results shown in Fig. 7 and Table 2 indicate that hybridization not only increases the flexural strength but also provides a significant increase in the flexural modulus for the entire group of hybrid composite specimens, when compared to the reference specimens made from single bamboo fiber [25]. By using equations 1-3, it can be seen that the 7th variation (V7) shows the highest flexural strength value of 288.5 MPa and the highest flexural modulus of 31.8 GPa. This is also reflected in the highest S/N ratio value, which is 49.20 dB for flexural strength (SNR A), followed by V2 and V4. While the highest variation in the S/N ratio value to flexural modulus (SBR B) is owned by V7, followed by V3 and V5. Thus, the V7 variation can be concluded as the most optimal combination in improving the mechanical performance of hybrid composites and will also be used in finite element simulation input.

To further contextualize the feasibility of the proposed hybrid composite, its mechanical performance was compared with standard materials commonly used for small fixed-wing UAV spars (≤ 2 m wingspan). Aluminum alloys are frequently employed as spar reinforcements in foam-based UAV wings due to their adequate stiffness and ease of fabrication, with a typical Young's modulus of approximately 69 GPa [26], [27]. For higher-performance UAV applications, Carbon Fiber Reinforced Polymer (CFRP) spars are predominantly utilized because of their superior stiffness-to-weight ratio, exhibiting elastic moduli generally ranging from 70 to 140 GPa depending on fiber orientation and volume fraction [28], [29].

In comparison, the optimized bamboo–carbon hybrid composite developed in this study achieved a flexural modulus of 31.8 GPa and a flexural strength of 288.5 MPa. Although the modulus of the hybrid composite is lower than that of conventional aluminum and CFRP systems, its stiffness remains within a structurally acceptable range for medium-load UAV configurations, particularly when combined with an optimized cross-sectional geometry, as demonstrated in the FEM analysis. Moreover, unlike fully synthetic CFRP systems, the bamboo–carbon hybrid composite offers partial renewability and reduced material cost, highlighting its potential as a more sustainable alternative for UAV spar structures.

3.3 The Signal-to-Noise (S/N) ratio response

Although the best variation has been identified, the analysis does not indicate which factors and levels most influence the mechanical response. Therefore, further analysis was conducted using the S/N Ratio method. Based on the S/N Ratio analysis for the flexural strength response (Fig. 8(a)), the factors that have the most significant influence on the test results are the stacking sequence, followed by the volume fraction and fiber ratio. This is in line with

previous studies [30], [31]. The highest S/N value was obtained with a combination of 60% volume fraction, a 40:60 bamboo fiber: carbon ratio, and a CBC stacking sequence. This combination produces the highest flexural strength value and demonstrates good yield stability against variations in the manufacturing process. This is due to the orientation of the CBC laminate, which places the carbon layer on the outside, thus being able to withstand maximum tensile and compressive stresses during flexural loading. Meanwhile, increasing the volume fraction to 60% also increases the density and effectiveness of stress transfer between layers.

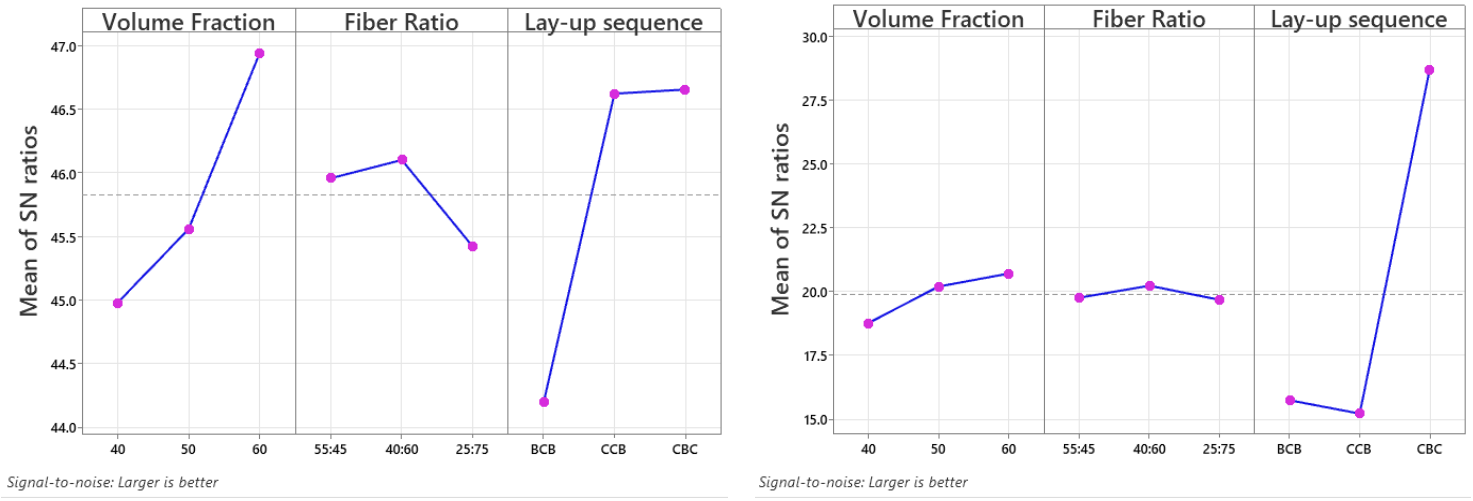

(a) (b)

Fig. 8. Analysis of S/N ratio based on three control factors—volume fraction, fiber ratio, and stacking sequence: (a) on flexural strength, (b) on flexural modulus

The S/N plot in Fig. 8(b) shows that the stacking sequence is the most dominant factor in influencing the flexural modulus, with the CBC configuration producing the highest S/N value and the most significant increase in response compared to BCB and CCB. The volume fraction factor also shows a positive trend, with the 60% level yielding a higher modulus than 40% and 50%. Meanwhile, in the fiber ratio factor, the 40:60 (bamboo: carbon) composition provides the highest S/N value, indicating that increasing the portion of carbon fiber contributes to stiffness, although the effect is not as large as the influence of the stacking sequence. To further evaluate the statistical significance of these factors, an Analysis of Variance (ANOVA) was conducted. Table 3 summarizes the ANOVA results evaluating the effects of volume fraction, fiber ratio, and stacking sequence on flexural strength.

Table 3. ANOVA values calculated based on control variable data for flexural strength

Control variable	DF	Adj SS	Adj MS	F-Value	P-Value
Volume fraction	2	7540	3770	1.55	0.226
Fiber ratio	2	680	340.1	0.14	0.870
Stacking sequence	2	30009	15004.3	6.15	0.005
Error	38	92654	2438.3		
Total	44	130883			

Based on the ANOVA results obtained using the General Linear Model (Table 3), the stacking sequence factor was found to have a significant effect on the flexural strength, with a P-value of 0.005, which is lower than the significance level of 0.05. In contrast, volume fraction and fiber ratio did not show a statistically significant effect, with P-values of 0.226 and 0.870, respectively.

The highest F-value was observed for the lay-up sequence factor (F = 6.15), indicating that this factor is the most dominant parameter influencing the flexural strength of the composite. This result suggests that the stacking sequence plays a critical role in determining the bending strength of the composite material.

Based on the main effect analysis in Figs. 8(a) and 8(b), each factor exhibits a distinct contribution to the flexural strength and flexural modulus responses. However, the optimal variation cannot be determined from a single parameter; therefore, a multi-response optimization approach is required. Therefore, the combined S/N values of flexural strength and flexural modulus were normalized and combined using equal weights (0.5:0.5) using the MPI method, as shown in Table 4.

Table 4. Results of variation analysis with the best response

Variants	Normalized strength	Normalized modulus	MPI (0.5:0.5)	Ranking
V1	0	0	0	9
V2	0.76	0.15	0.46	6
V3	0.61	0.92	0.77	**2**
V4	0.75	0.25	0.50	4
V5	0.41	0.84	0.63	**3**
V6	0.44	0.23	0.33	7
V7	1.00	1.00	1.00	**1**
V8	0.64	0.33	0.48	5
V9	0.49	0.08	0.29	8

The MPI calculation results show that variation V7 obtained the highest value (MPI = 1.00), thus categorizing it as the most optimal configuration, as it provides the best combination of flexural strength and stiffness. This finding confirms that composite material selection should not be based solely on maximum strength but must consider the simultaneous nature of both mechanical properties, particularly for structural applications operating under repeated flexural loading conditions, such as UAV wing spars.

Thus, the V7 variation was determined as the most superior material design candidate, and was subsequently used as a material input in FEM-based numerical simulations to validate its structural performance under actual loading conditions in the spar component.

3.4 Finite element simulation results

After obtaining the composite variation with the best flexural performance through experimental testing and Taguchi optimization, the next stage is to conduct a numerical analysis based on the FEM. This simulation aims to validate the behavior of the selected material (V7) when applied to the UAV spar component with three different cross-sectional configurations, so that not only the material, but also the influence of the geometric design on the structural strength can be analyzed.

A numerical model is built by inputting material parameters from flexural tests. Loading conditions and boundary conditions are made to represent the operational behavior of the spar component when installed on the UAV wing structure. The selection of subsequent evaluation parameters is based on the match between the simulation output and the failure mechanisms that occur in the composite material during the flexural test.

Maximum principal stress is chosen because it is the most appropriate failure parameter for anisotropic composite materials,

represents the maximum tensile stress in the fiber layer, and is in line with the experimental data of flexural strength used for validation. Then, the maximum principal elastic strain is chosen because it is able to represent the maximum tensile deformation in the fiber direction, is in line with experimental data based on flexural strain, and is in accordance with the theory of strain-based composite failure.

Fig. 9 shows the distribution of maximum principal stress in a circular spar structure resulting from static simulations. The maximum stress value recorded was 264.3 MPa and was localized at the bottom of the spar in the area around the center support, which represents the connection between the spar and the fuselage. Unlike the three-point loading scheme in laboratory testing, this simulation configuration follows the actual conditions of a fixed-wing UAV, where aerodynamic loading occurs at both ends of the spar (wingtips), while the fuselage is in the middle and acts as the main support. The high stress concentration in the center support area occurs due to the large force reaction at that point, resulting in maximum bending moments and tensile strains in the bottom fibers of the spar. This stress pattern is consistent with structural mechanics theory for beams with two distributed loads at the ends and a center support, and is in line with the results of previous studies on composite wing structures [32], [33], [34], which also reported that the critical point of failure actually occurred at the root joint or interface with the fuselage, not at the wingtip.

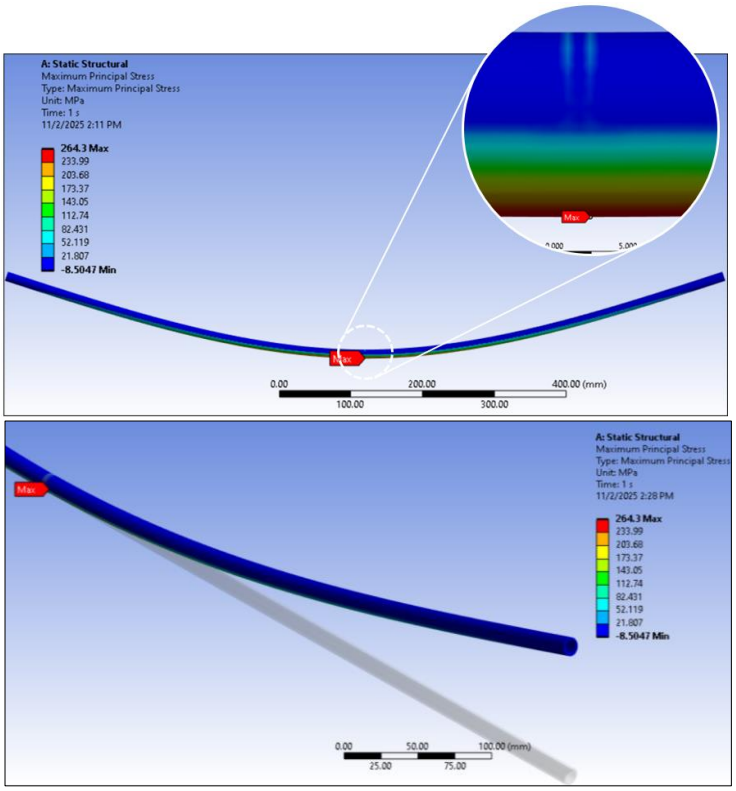

Fig. 9. Distribution of principal stress on a circular cross-section spar

In contrast to the previous results, Figs. 10 and 11 show a much lower maximum principal stress distribution, approximately 134 MPa for the W-shaped cross-section and 125 MPa for the hollow square cross-section. This stress reduction indicates that geometry modifications significantly impact the spar's ability to distribute loads and reduce stress concentrations. In both models, the maximum stress still occurs at the bottom of the spar, located directly in the center zone.

The difference in stress values between the figures is due to variations in cross-section shape, which affect the cross-section's moment of inertia. The greater the moment of inertia, the lower the bending stress under the same load.

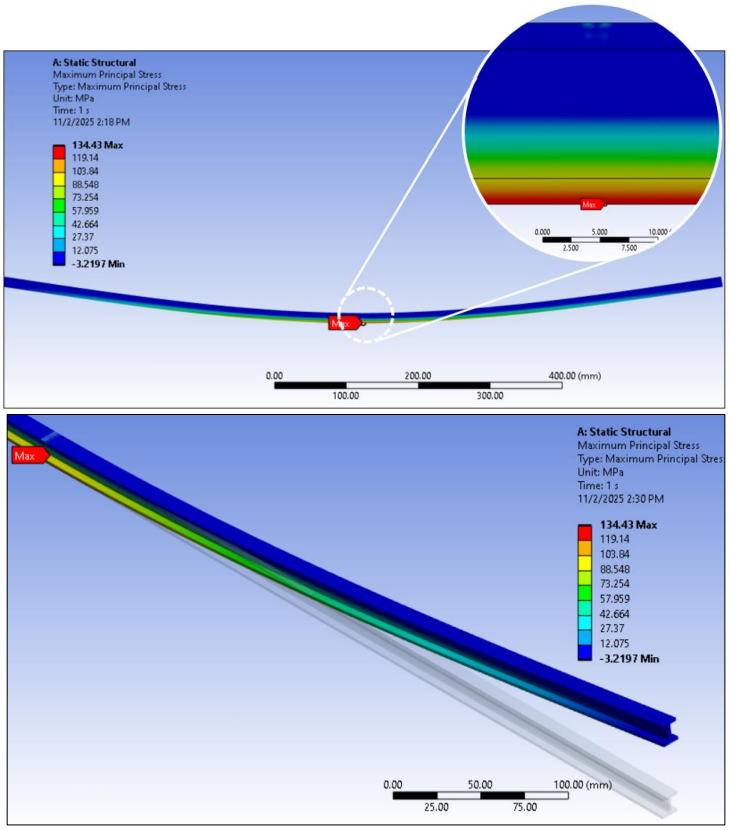

Fig. 10. Distribution of principal stress on a W-shaped spar

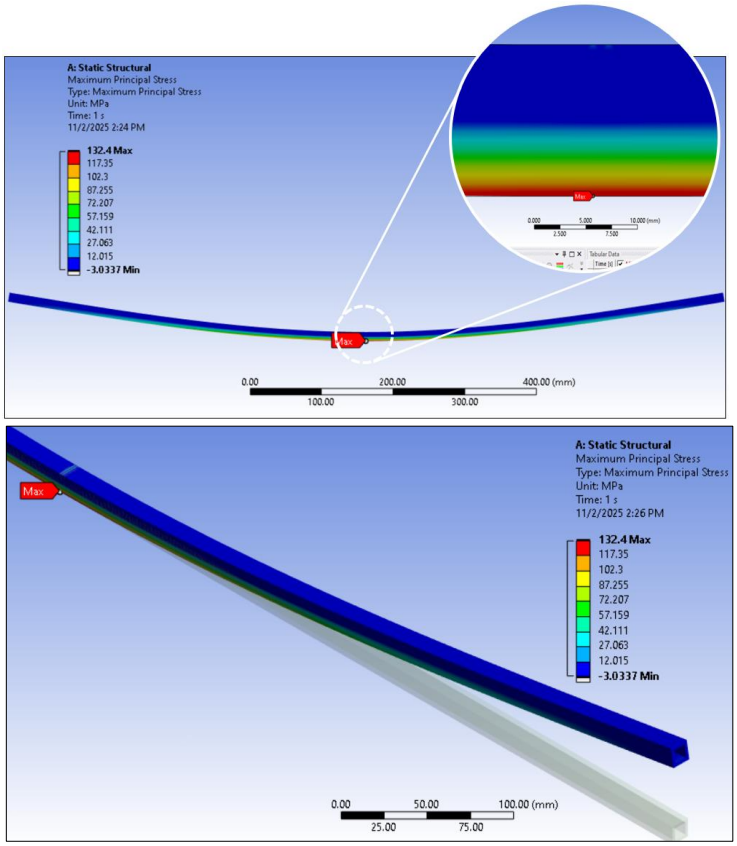

Fig. 11. Distribution of principal stress on a hollow square cross-section spar

Therefore, geometries with material distribution farther from the neutral axis tend to have lower maximum stresses. These results demonstrate that optimizing the cross-section shape is an effective way to reduce peak loads without changing materials or manufacturing processes.

The maximum principal elastic strain values obtained from the three cross-sectional models show quite significant differences (Table 5). In the circular cross-section, the maximum principal elastic strain was recorded at 0.008316 mm/mm, which is the highest value among all variations. This indicates that the circular geometry

has the lowest flexural stiffness, thus experiencing the largest deformation under the same loading conditions. In contrast, the W-shape and hollow square cross-sections showed lower maximum strain values, at 0.0042278 mm/mm and 0.0041634 mm/mm, respectively, indicating a stiffer and more stable deformation response.

Table 5. Simulation results and SF calculations data

Cross-sectional shape	Max. principal stress (MPa)	Max. principal elastic strain (mm/mm)	SF	Ranking
Hollow circular	264.3	0.008316	1.09	3
W-shape	134	0.0042278	2.15	2
Hollow square	125	0.0041634	2.18	1

To evaluate the structural feasibility of each spar section design, a Safety Factor (SF) was calculated based on simulation results. The primary objective of determining the SF is to assess the extent to which the model remains within safe limits before reaching the material failure stress, thus determining whether the design is feasible for use without experiencing structural failure during operation. At this stage, the SF analysis focused solely on the maximum principal stress value. Because flexural failure in composites is primarily triggered by maximum tensile stress in the fiber direction, a stress-based approach is therefore sufficiently representative for the initial assessment.

The SF calculation was performed using a simple equation: dividing the experimental flexural strength value by the maximum principal stress value from the simulation. With the SF values obtained for each geometry variation (Table 5), the next step was to interpret the results to determine which section design provides the most adequate structural safety margin. The SF for the hollow circular section was 1.09. This value indicates conditions approaching the ultimate limit (a very small safety margin). This section possesses a risk when used under current service load conditions (especially if stress concentrations or impulse/fatigue loads are present). In contrast, the W-shaped and hollow-square sections had SFs of 2.15 and 2.18, respectively, indicating a safer and more stable structural capacity for quasi-static loads.

Based on these results, the hollow-square section not only provided the highest safety factor but was also consistent with previous evaluation results (stress, strain, and deformation distribution), thus concluding it as the most optimal spar geometry in this study.

4 Conclusions

This research determined the material variations and spar cross-section designs that provide optimal mechanical performance for UAV wing structure applications. Through flexural testing and Taguchi analysis, the V7 bamboo–carbon hybrid composite configuration (60% volume fraction, 40:60 fiber ratio, and CBC stacking sequence) demonstrated the best performance, with a flexural strength of 288.5 MPa and a flexural modulus of 31.8 GPa, while also producing the highest S/N ratios for both responses. From the simulation analysis of stress, strain, and safety factor, it was found that the hollow circular cross-section had a low safety margin (SF = 1.09), while the W-shaped and hollow-square cross-sections demonstrated significantly safer responses, with safety factors of 2.15 and 2.18, respectively. Based on the overall evaluation, the hollow-square design was determined to be the most optimal geometric configuration due to its lowest working stress, minimal deformation, and highest structural safety. These results demonstrate that bamboo–carbon hybrid composites are not only viable as alternative materials for UAV spar structures, but also capable of providing competitive mechanical performance with pure synthetic composites, with the added advantage of potential material sustainability.

Acknowledgements

The authors would like to acknowledge the financial support from the Universitas Malikussaleh through the 2025 PNBP Research Grant Program, under contract number 120/PPL-2/SWK-II/AL.04/2025.

References

[1] Statista Market Forecast, "consumer electronics drones southeast-asia," https://www.statista.com/outlook/cmo/consumer-electronics/drones/southeast-asia. Accessed: Jan. 28, 2025. [Online]. Available: https://www.statista.com/outlook/cmo/consumer-electronics/drones/southeast-asia

[2] Z. Yahya, D. E. Mujahiddin, R. Setiawan, and A. P. Sujalu, "The Utilised Unmanned Aerial Vehicles in Forest Plantation Maintenance," *Jurnal Penelitian Pendidikan IPA*, vol. 11, no. 9, pp. 527–532, Oct. 2025, doi: 10.29303/jppipa.v11i9.12623.

[3] N. Nurdin *et al.*, "Precision Aquaculture Drone Mapping of the Spatial Distribution of Kappaphycus alvarezii Biomass and Carrageenan," *Remote Sens. (Basel).*, vol. 15, no. 14, p. 3674, Jul. 2023, doi: 10.3390/rs15143674.

[4] S. E. Putri, Fitriani, Sukmasari, Willy, Periawan, and P. R. Hukul, "Analisis Pemanfaatan Drone Untuk Pemantauan Illegal Fishing Di Perairan," *Jurnal Perikanan dan Kelautan*, vol. 1, no. 1, pp. 37–43, Dec. 2024, doi: 10.70134/peraut.v1i1.318.

[5] K. Raja Sekar, M. Ramesh, R. Naveen, M. S. Prasath, and D. Vigneshmoorthy, "Aerodynamic design and structural optimization of a wing for an Unmanned Aerial Vehicle (UAV)," *IOP Conf. Ser. Mater. Sci. Eng.*, vol. 764, no. 1, p. 012058, Feb. 2020, doi: 10.1088/1757-899X/764/1/012058.

[6] R. Kirubakaran, D. Lokesharun, S. Rajkumar, and R. Anand, "Aircraft Wing Weight Optimization by Composite Material Structure Design Configuration," *IOSR Journal of Mechanical and Civil Engineering (IOSR-JMCE) e-ISSN*, vol. 14, no. 6, pp. 71–80, 2017, doi: 10.9790/1684-1406027180.

[7] N. L. Aung, O. Tatarnikov, and P. W. Aung, "Optimization of composite wing spars for an unmanned aerial vehicle," *IOP Conf. Ser. Mater. Sci. Eng.*, vol. 971, no. 5, p. 052076, Nov. 2020, doi: 10.1088/1757-899X/971/5/052076.

[8] M. A. Yilmaz, K. Hasirci, B. Gündüz, and A. B. Irez, "Advanced composite wing design for next-generation military UAVs: A progressive numerical optimization framework," *Defence Technology*, vol. 48, pp. 141–155, Jun. 2025, doi: 10.1016/j.dt.2025.02.020.

[9] *V International Scientific and Theoretical Conference «Scientific review of the actual events, achievements and problems»*. Primedia E-launch LLC, 2025. doi: 10.36074/scientia-03.10.2025.

[10] M. Milewski, J. Wróbel, A. Kierzkowski, and D. Vališ, "Experimental and numerical modal analysis of an unmanned aerial vehicle's composite wing," *Simul. Model. Pract. Theory*, vol. 142, p. 103106, Jul. 2025, doi: 10.1016/j.simpat.2025.103106.

[11] M. Oliveira, V. Neves, and M. D. Banea, "Mechanical and Thermal Characterization of Bamboo and Interlaminar Hybrid Bamboo/Synthetic Fibre-Reinforced Epoxy Composites," *Materials*, vol. 17, no. 8, p. 1777, Apr. 2024, doi: 10.3390/ma17081777.

[12] S. M. Ahmad, M. C. Gowrishankar, and M. Shettar, "A review on properties of bamboo fiber polymer composites and bamboo/glass fiber/nanoclay hybrid composites," *Mater. Res. Express*, vol. 12, no. 1, p. 012002, Jan. 2025, doi: 10.1088/2053-1591/ada875.

[13] K. M. F. Hasan *et al.*, "Sustainable bamboo fiber reinforced polymeric composites for structural applications: A mini review of recent advances and future prospects," *Case Studies in Chemical and Environmental Engineering*, vol. 8, p. 100362, Dec. 2023, doi: 10.1016/j.cscee.2023.100362.

[14] S. Kore *et al.*, "Performance of hybridized bamboo-carbon fiber reinforced polypropylene composites processed using wet laid technique," *Composites Part C: Open Access*, vol. 6, p. 100185, Oct. 2021, doi: 10.1016/j.jcomc.2021.100185.

[15] F. R. Benthony, S. Suluh, C. S. A. Gusti, and A. Ariyanto, "Enhancing mechanical strength of petung bamboo (dendrocalamus asper) composites using brackish water immersion," *Jurnal Polimesin*, vol. 23, no. 3, p. 367, Jun. 2025, doi: 10.30811/jpl.v23i3.6219.

[16] M. Benarioua *et al.*, "Statistical Normalization of Mechanical Properties of Natural Date Palm Biofibers Using the Box-Cox Transformation," *Journal of Natural Fibers*, vol. 22, no. 1, Dec. 2025, doi: 10.1080/15440478.2025.2544176.

[17] B. Mohamad, S. Amroune, R. Miri, A. Benchekkour, and K. Galoyan, "Design optimization methodology of submarine using multilevel numerical CFD models," *FME Transactions*, vol. 53, no. 2, pp. 280–288, 2025, doi: 10.5937/fme2502280B.

[18] R. Prabhu, S. Mendonca, P. K. Bellairu, R. D'Souza, and T. Bhat, "Impact of stacking sequence on mechanical and dry sliding wear properties of bamboo and flax fiber reinforced hybrid epoxy composite filled with TiO_2 filler," *Multidiscipline Modeling in Materials and Structures*, vol. 20, no. 6, pp. 1180–1191, Oct. 2024, doi: 10.1108/MMMS-07-2024-0193.

[19] H. Sosiati, Hidayatullah, and S. Hamdan, "Effect of Woven E-glass and Bamboo Stacking Sequences on the Properties of Laminated Composites Using Polyester Matrix Filled with Eggshell Microparticles," *Evergreen*, vol. 11, no. 2, pp. 693–700, Jun. 2024, doi: 10.5109/7183343.

[20] Z. Wang, L. Wang, F. Tang, and C. Shen, "PLA-Based Composite Panels Prepared via Multi-Material Fused Filament Fabrication and Associated Investigation of Process Parameters on Flexural Properties of the Fabricated Composite," *Polymers (Basel).*, vol. 16, no. 1, p. 109, Dec. 2023, doi: 10.3390/polym16010109.

[21] M. Darsin, R. R. Mauludy, I. Hardiatama, B. A. Fachri, M. E. Ramadhan, and D. Parningotan, "Analysis of the effect 3D printing parameters on tensile strength using Copper-PLA filament," *SINERGI*, vol. 26, no. 1, p. 99, Feb. 2022, doi: 10.22441/sinergi.2022.1.013.

[22] I. R. Chowdhury, N. H. Nash, A. Portela, N. P. O'Dowd, and A. J. Comer, "Analysis of failure modes for a non-crimp basalt fiber reinforced epoxy composite under flexural and interlaminar shear loading," *Compos. Struct.*, vol. 245, p. 112317, Aug. 2020, doi: 10.1016/j.compstruct.2020.112317.

[23] C. Breite *et al.*, "Detailed experimental validation and benchmarking of six models for longitudinal tensile failure of unidirectional composites," *Compos. Struct.*, vol. 279, p. 114828, Jan. 2022, doi: 10.1016/j.compstruct.2021.114828.

[24] H. Sadaghian, M. Pourbaba, S. Zeinali Andabili, and A. Mirmiran, "Experimental and numerical study of flexural properties in UHPFRC beams with and without an initial notch," *Constr. Build. Mater.*, vol. 268, p. 121196, Jan. 2021, doi: 10.1016/j.conbuildmat.2020.121196.

[25] T. Srinag *et al.*, "Flexural and impact response of bamboo and pineapple leaf fiber reinforced composites using experimental and numerical techniques," *International Journal on Interactive Design and Manufacturing (IJIDeM)*, vol. 18, no. 5, pp. 3383–3395, Jul. 2024, doi: 10.1007/s12008-023-01564-6.

[26] P. M. N. Araujo, T. R. Costa, and E. C. Silva, "Design And Manufacturing Process Of A Uav Composite Wing Spar," in *Proceedings of the 4th Brazilian Conference on Composite Materials*, Pontifícia Universidade Católica do Rio de Janeiro, 2018, pp. 562–569. doi: 10.21452/bccm4.2018.09.06.

[27] N. L. Aung, O. Tatarnikov, and P. W. Aung, "Optimization of composite wing spars for an unmanned aerial vehicle," *IOP Conf. Ser. Mater. Sci. Eng.*, vol. 971, no. 5, p. 052076, Nov. 2020, doi: 10.1088/1757-899X/971/5/052076.

[28] Y. Huang *et al.*, "3D printing of topologically optimized wing spar with continuous carbon fiber reinforced composites," *Compos. B Eng.*, vol. 272, p. 111166, Mar. 2024, doi: 10.1016/j.compositesb.2023.111166.

[29] A. Ullah, M. N. Ahmed, and B. Saeed, "Optimizing UAV Wing Performance: A Computational Analysis with Computer-Based Algorithms for Composite Material Integration," *International Journal of Innovations in Science and Technology*, pp. 287–300, Mar. 2024, doi: 10.33411/ijist/202461287300.

[30] Z. Wang, L. Wang, F. Tang, and C. Shen, "PLA-Based Composite Panels Prepared via Multi-Material Fused Filament Fabrication and Associated Investigation of Process Parameters on Flexural Properties of the Fabricated Composite," *Polymers (Basel).*, vol. 16, no. 1, p. 109, Dec. 2023, doi: 10.3390/polym16010109.

[31] T. A. Miliket, M. B. Ageze, M. T. Tigabu, and M. A. Zeleke, "Experimental characterizations of hybrid natural fiber-reinforced composite for wind turbine blades," *Heliyon*, vol. 8, no. 3, p. e09092, Mar. 2022, doi: 10.1016/j.heliyon.2022.e09092.

[32] R. Kumpati, W. Skarka, and M. Skarka, "Design optimization and failure analysis of natural composite sandwich T-joints under pulling load conditions," *Eng. Fail. Anal.*, vol. 164, p. 108672, Oct. 2024, doi: 10.1016/j.engfailanal.2024.108672.

[33] X. Yuan, Q. Li, and D. Gong, "Design of the stringer end of the composite centre wing lower panel in the plug-in butt joint form," *J. Phys. Conf. Ser.*, vol. 1827, no. 1, p. 012102, Mar. 2021, doi: 10.1088/1742-6596/1827/1/012102.

[34] U. Tariq and F. Mazhar, "Static Structural Analysis of Fighter Aircraft's Wing Spars," in *2021 International Bhurban Conference on Applied Sciences and Technologies (IBCAST)*, IEEE, Jan. 2021, pp. 221–243. doi: 10.1109/IBCAST51254.2021.9393241.